SUPPLEMENTARY FIGURES

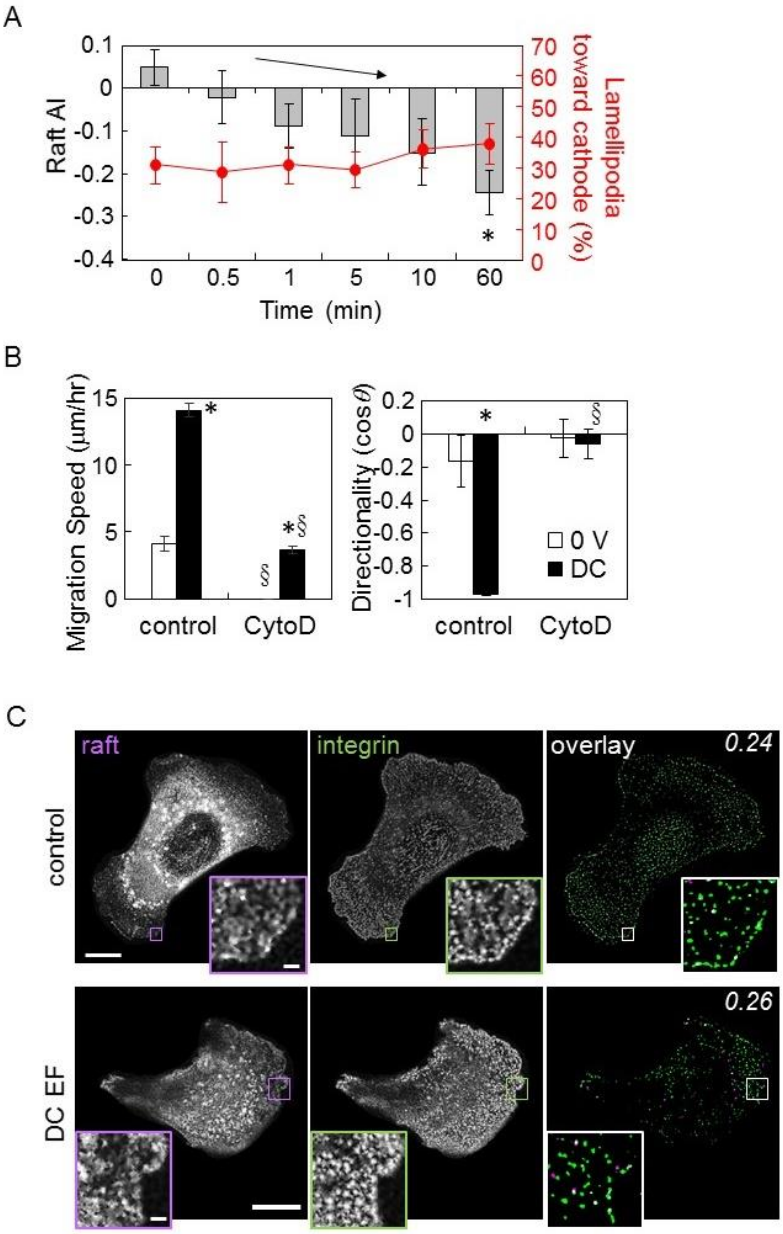

Figure S1 (A) Temporal response of lipid raft and lamellipodia extension to applied DC EF in fibroblasts (n=12-58, *p<0.03 vs t=0, arrow indicate a trend of decrease for raft distribution, p<0.001, no significant difference were found in lamellipodia extension). (B) Cytochalasin treatment inhibits cell migration and directionality (n=20-65, *p<0.001 vs 0V, §p<0.001 vs control). (C) STED microscopy images of representative cells dual labeled with raft and integrin. Scale bar = 10 μm, insert scale bar = 1 μm. Values in the top right corner of the overly image indicate the average Mander's colocalization coefficient for integrin overlap with raft.

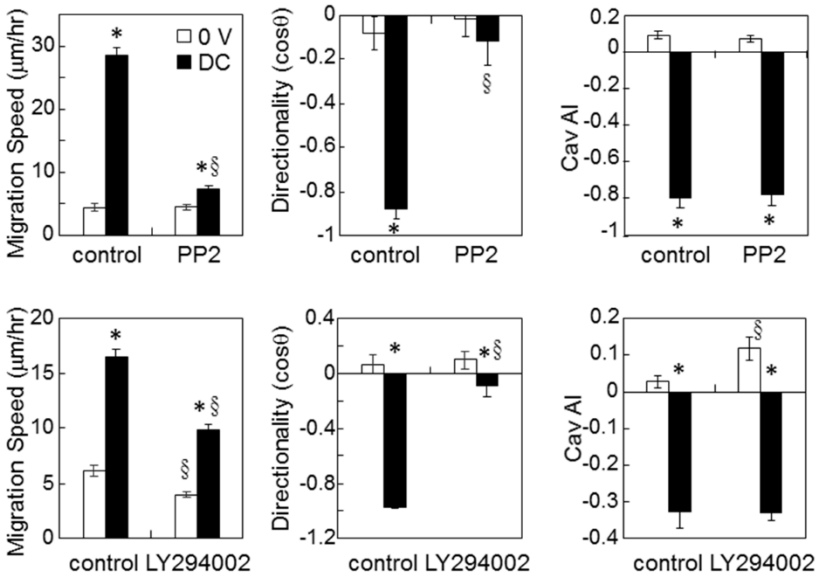

Figure S2 Inhibition of PI3K and Src (with LY294002 and PP2 respectively) attenuated cell migration speed and abolished cell directionality in applied EF, while having no effect on caveolin polarization (n>50 for all migration and n>15 for all AI measurements, *p<0.05 vs 0V, §p<0.01 vs control).

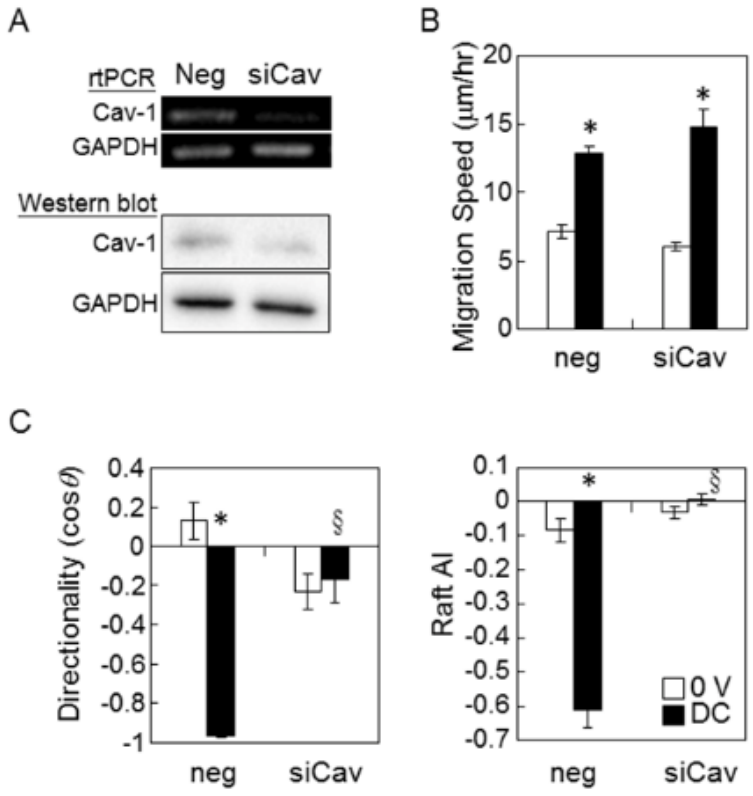

Figure S3 (A) Suppression of Cav gene and protein expression with siRNA. (B) Cav knockdown had minimal effects on cell migration speed (n=40-95, $p<0.001$ vs 0V). (C) Cholesterol replenishment with 0.25 mM cholesterol and 2.5 mM MβCD did not alter the effects of siCav on cell directionality and raft redistribution in EF (n=47-69 for migration and 25-39 for raft distribution, *$p<0.001$ vs 0V, §$p<0.001$ vs neg)

SUPPLEMENTARY INFORMATION

Detailed Materials and Methods

Cell Culture

All reagents are purchased from Invitrogen (NY, USA) unless otherwise noted. Anterior cruciate ligament (ACL) explants were harvested from freshly slaughtered young pigs and cultured in DMEM supplemented with 10% FBS until confluence. Human bone marrow-derived mesenchymal stem cells (MSCs) were kindly provided by Dr. Shih-Chieh Hung (1). For all studies, MSCs were used at passages 11-20. Human lung adenocarcinoma cell lines CL1–5 and CL1–0 were kindly provided by Dr. Pan-Chyr Yang and used at passages 5-10 (2). For electric field stimulation studies, cells were seeded on sterile glass slides at 10^4 cells/cm^2 for two hours.

Fluorescence Imaging

Alexa Fluor 555 conjugate-cholera toxin B (CTxB, Invitrogen) was used to label the GM1 gangliosides in lipid rafts. CTxB was diluted with chilled complete growth medium at 1 μg/ml. After EF stimulation, cells were rinsed with chilled medium and treated with CTxB for 10 minutes on ice before formalin fixation and immediately imaged. STED measurements were done with fixation prior to CTxB incubation unless otherwise noted. Due to the multivalent nature of CTxB, raft sizes increased when cells were incubated with CTxB prior to fixing (CTxB incubation after fixation: 0.028±0.005 μm^2, CTxB incubation before fixation: 0.032±0.007 μm^2, n=17-24, p=0.04), however, similar results in raft polarization were observed when cells were fixed prior to CTxB labeling (p=0.69). For other labeling, cells were fixed and permeabilized before incubating overnight with the primary antibodies for β1 integrin (Millipore, MA, USA), phospho-cav1 (Cell Signaling, MA, USA), phosphor-src (Cell Signaling), PI3K (Millipore), or RhoA (Cytoskeleton, CO, USA). Images were acquired with epifluorescence microscopy and analyzed using a custom LabView program (National Instruments, TX, USA).

Inhibition and Knockdown Studies

Cholesterol depletion was achieved by treating the cells with 5 mM methyl β-cyclodextrin (MβCD, Sigma, MO, USA, (3)) for one hour in serum-free DMEM. To increase membrane cholesterol content, 1 mM cholestryl hemisuccinate (Sigma, MO, USA) was applied for 30 minutes (4). Cytochalasin B (Cayman Chemical, MI, USA) suppressed actin polymerization at 5 μg/mL for one hour. Src activity was inhibited with PP2 (Calbiochem, CA, USA) at 1 μg/mL for two hours. LY294002 (Calbiochem)

was used to inhibit PI3K activity at 10 μg/mL for one hour in serum-free medium. Functional blocking antibody for α2β1 integrin (clone BHA2.1, Millipore) was applied for 30 minutes to inhibit integrin signaling (5). siRNA was used to knockdown caveolin-1 (Cav-1) expression levels (5'-AAGAAUUUGAAUUUAUUCCAG-3', Qiagen, CA, USA). 150 ng si-Cav1 or 75 ng negative control siRNA were transfected using the HiPerFect reagent (Qiagen) two days before EF stimulation.

Super-resolution Imaging

Super-resolution imaging was achieved with stimulated emission depletion (STED) microscopy on a LEICA TCS SP5 STED system. Lipid rafts were labeled with AlexaFlour 488 conjugate-CTxB (Invitrogen) after formalin fixation. Primary antibody for active β1 integrin was purchased from Abcam (clone 12G10) and fluorescently labeled with the STAR 440SXP secondary antibody (Abberior). Raft sizes were analyzed by a custom Matlab program based on an adaptive thresholding algorithm after background noise removal. Integrin and raft colocalization was calculated using a similar method for the fraction of integrin intensity in the raft regions, based on Mander's method (6).

Modeling of Lipid Rafts in Response of Applied Electric Fields

Modeling Drift Velocity of Lipid Rafts in Membranes

Figure 1 illustrates a lipid raft with a cylindrical portion *M* embedded in the membrane and a cylindrical portion *A* extending in external solution. When an electric field is applied, three forces are considered to act on this lipid raft (7-9): the electrical force due to an external electric field (F_E) (10), the hydrodynamic force resulting from the aqueous medium (F_{HA}) (11), and the drag force in membrane (F_{DM})(12). Drift velocity of the lipid raft at steady state can be obtained by setting the sum of all forces exerting on the lipid raft equal to zero, as shown in Equation 1. The drift velocity can be obtained by expressing F_E, F_{HA}, and F_{DM} in the forms with lipid raft velocity, as shown in the following sections.

$$\vec{F}_{HA} + \vec{F}_{DM} + \vec{F}_E = 0 \quad (1)$$

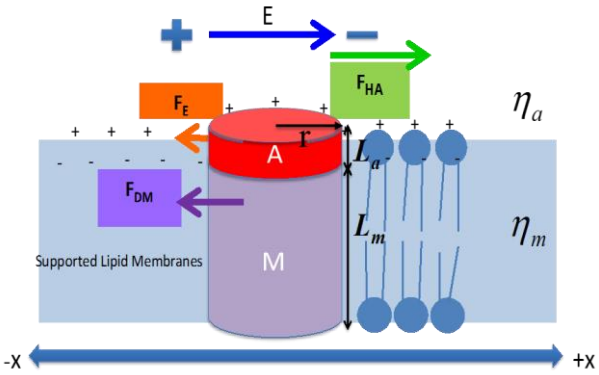

Figure 1. Model of a lipid raft in an electric field (E). The portion A is the portion of lipid raft in the aqueous medium, and the portion M is embedded in the membrane. F_E is the electrical force on lipid raft due to the external electric field, F_{HA} is the hydrodynamic force on lipid raft from the aqueous medium, and F_{DM} is the drag force from the membrane.

(i) Hydrodynamic Force due to the Aqueous Medium (F_{HA})

The hydrodynamic force (F_{HA}) on lipid raft results from the flow of the aqueous medium induced by electro-osmotic flow. The force on the hydrophilic part of the raft is equal to the associated drag coefficient times the velocity of the flow with respect to the lipid raft (11, 13).

$$\overrightarrow{F_{HA}} = d(r)(\vec{V}_{EOF} - \vec{V}) \qquad (2)$$

where $\vec{V}$ is the velocity of the lipid raft, $\vec{V}_{EOF}$ is the velocity of the electro-osmotic flow, and *d(r)* is the portion A-associated drag coefficient as a function of lipid raft radius (r). The drag coefficient *d(r)* is related to the shape, size and orientation of portion A with respect to the aqueous flow (11, 13) and is obtained by using COMSOL Multiphysics software. For the cylindrical portion A with a height of 1 nm, we can obtain d(r)[kg/s] = $2\text{x}10^{-11}$ ln(r [m]) + $5\text{x}10^{-10}$. Velocity of the electro-osmotic flow can be expressed as Equation 3.

$$\vec{V}_{EOF} = \frac{-\varepsilon_0 \varepsilon_r \zeta_{EOF} \vec{E}}{\eta_a} \qquad (3)$$

where ε_0 is the permittivity of free space, ε_r is the dielectric constant of the medium, and ζ_{EOF} is the zeta potential of the membrane surface.

(ii) Drag Force from the Lipid Membrane (F_{DM})

Drag force exerted by the lipid membrane on portion M of the lipid raft is equal to the portion M-associated drag coefficient times the velocity of the lipid membrane with respect to the lipid raft (12, 14), as shown in Equation 4. The portion M-associated drag force coefficient, g(r), can be obtained by using the Saffman-Delbrück approximation (14-16).

$$\overrightarrow{F_{DM}} = g(r)(\vec{V}_{membrane} - \vec{V}) \qquad (4)$$

where $g(r) = \frac{4\pi\eta_m\left[1-\left(\frac{\epsilon^3}{\pi}\right)\ln\left(\frac{2}{\epsilon}\right)+\frac{c_1\epsilon^{b_1}}{\left(1+c_2\epsilon^{b_2}\right)}\right]}{\ln\left(\frac{2}{\epsilon}\right)-\gamma+\frac{4\epsilon}{\pi}-\left(\frac{\epsilon^2}{2}\right)\ln\left(\frac{2}{\epsilon}\right)}$

and $\epsilon = \frac{2r_m\eta_a}{\eta_m}$

r is the lipid raft radius, η_m is the membrane viscosity, γ=0.577215, b_1=2.74819, b_2=0.61465, c_1=0.73761, and c_2=0.52119.

(iii) Force due to the Electric Field (F_E)

The Helmholtz-Smoluchowski equation (10) shows that the electrical force exerted on lipid rafts by the external electric field can be expressed as:

$$\overrightarrow{F_E} = \frac{d(r)\varepsilon_0\varepsilon_r\zeta_{EOF}\vec{E}}{\eta_a} \qquad (5)$$

where r is radius of lipid raft, ε_0 is permittivity of free space, ε_r is dielectric constant of the medium, ζ_a is zeta potential of protein, $\vec{E}$ is electric field (V/m), d(r) is aqueous

medium-lipid raft drag coefficient, and η_a is viscosity of the aqueous medium.

(iv) Drift Velocity of Lipid Raft

After obtaining the expressions of F_E, F_{HA}, and F_{DM}, we can substitute them into Equation 1 to obtain the drift velocity of lipid raft. Definitions of the symbols can be found in Equations 2-5 and Table 1.

$$\vec{V} = \frac{\frac{d(r)\varepsilon_0\varepsilon_r(\zeta_a-\zeta_{EOF})\vec{E}}{\eta_a}}{d(r)+g(r)} \qquad (6)$$

Algorithm to calculate migration displacement with time

In this study, size of lipid raft grows with time and electric field magnitude and direction also vary with time when an AC electric field is applied, which complicates the calculation of lipid raft displacement. We use a quasi-steady state approach which assumes that the steady state velocity shown in Equation 2 can be reached immediately at every time point with the corresponding electric field provided at that time. To calculate the displacement, we discretize the time space into small time intervals (10^{-5} sec) and use Matlab software to calculate the velocity at each time points, as shown in Equation 3. Integrating Equation 3 gives us the overall displacement.

$$\mathrm{x}_{i+1} = \mathrm{x}_i + \vec{V_l}(\mathrm{t}_{i+1} - t_i) \qquad (3)$$

where $\vec{V_l}$ is the lipid raft velocity at time t_i. x_i and x_{i+1} are the locations of the lipid raft at time t_i and t_{i+1}, respectively.

As for the model setting, we assume that lipid rafts are always in cylindrical shape with a height of 4 nm in the membrane (portion M) and a height of 1 nm in the aqueous medium (portion A). Initial lipid raft radius is set at 8 nm and increases every time upon collision. In the calculation algorithm, we assume lipid raft volume doubled upon merging of two identical lipid rafts while the cylinder height is kept the same and therefore the radius became the square root of two of the original value. Merge frequency is set to be half of the previous frequency after each merger and the initial merge frequency is set at 50 Hz. The merge frequency decreases with time because the overall number of lipid rafts and therefore the collision frequency decreases with time. Direction of the electric field (from the cathode to anode) is set as the positive direction, as shown in Figure 1. All of the other parameters used during the calculations are shown in Table 1. The AC electric field frequency is specified according to the experiments.

Table 1. Parameters and values used to calculate lipid raft displacement. (17-22)

Parameters	Description	Value
L_a	Height of portion A	1 nm
L_m	Height of portion M	2 nm
η_a	Viscosity of aqueous phase	$1x10^{-3}$ kg/m s
η_m	Viscosity of lipid membrane	$2x10^{-10}$ kg/s
r_0	Initial radius of lipid raft	8 nm
r_{max}	Maximum radius of lipid raft	1 μm
ζ_a	Zeta potential of lipid raft	-10mV
ξ_{EOF}	Zeta potential of membrane surface	-60mV
ε_0	Permittivity of free space	$8.854*10^{-12}$ F/m
ε_r	Dielectric constant of medium	80.1
E	Electric field magnitude	120 V/cm

The Displacement of a Radius-Increasing Lipid Raft in DC or AC Electric Fields.

Figure 2 shows the model-predicted displacement situations of a radius-increasing lipid raft when a DC or an AC electric field is applied to lipid raft. To illustrate how the growing of lipid raft can influence the displacement, we only show the early situation (0-5 sec). When a 120 V/cm DC electric field is applied, lipid raft can migrate toward the electric field direction until the lipid raft reaches cell boundary. The velocity, the slope of displacement, decreases with time due to increasing lipid raft radius (Figure 2(a)). When a 120 V/cm AC electric field is applied, lipid raft can have oscillatory migration (Figure 2(b)). Since lipid raft size grows and drift velocity drops with time, lipid raft can balance at a certain location in the AC electric field. When lipid raft grows randomly with respect to the AC field oscillation, the balanced location should be roughly in the middle of maximum displacement. If lipid raft grows more often or grows to a critical size when the AC field is positive or negative, the balanced location should be toward the positive or negative pole.

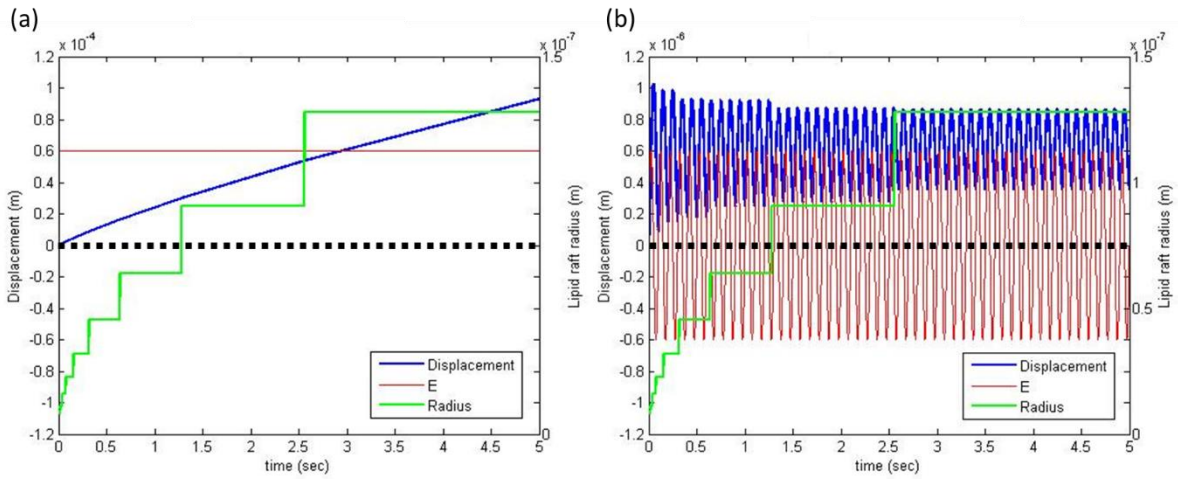

Figure 2. Possible displacement situations of a growing lipid raft (a) when a 120 V/cm DC electric field is applied; and (b) when a 120 V/cm AC electric field is applied. Left y-axis and blue line: displacement of a lipid raft (x). Right axis and green line: lipid raft radius (r). Dashed line: original location of the lipid raft (x=0) and zero line of electric field. Red line: the applied electric field (above the dashed black line, the electric field is positive and vice versa).

AC Electric Field Frequency Influences the Displacement Magnitude.

Since direction of lipid raft drift velocity is always the same as the electric field direction ($\zeta_a > \zeta_{EOF}$), the maximum displacement for the lipid raft is within the duration of a half wavelength of the sinusoidal AC electric field before the field changes direction. Therefore, if AC frequency is small, the duration for lipid raft to migrate is small and the maximum displacement is small. Figure 3 shows the displacement situations when we change the AC frequency from 10 Hz to 100 Hz while keeping all of the other parameters constant (Table 1). AC frequency at 10 Hz provides more time for the lipid raft to migrate before velocity direction is changed and therefore allows the lipid raft to have a larger displacement than 50 and 100 Hz. In addition, the duration for 10 Hz is around five times that of 50 Hz and ten times 100 Hz, and therefore the maximum displacement of 10 Hz is also around five and ten times the maximum magnitude of the 50 Hz and 100 Hz.

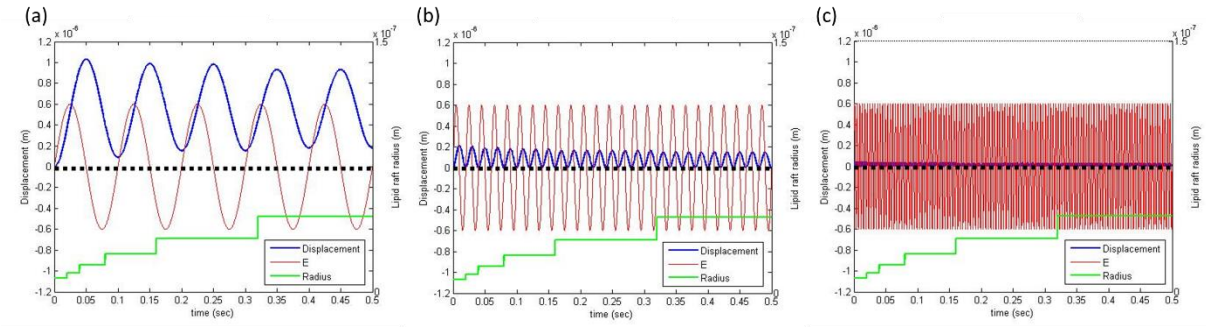

Figure 3. Predicted displacement situations when the 120 V/cm AC electric field has a frequency of (a) 10 Hz (b) 50 Hz and (c) 100 Hz. Symbols, lines and axes are the same as those in Figure 2.

Constrained Lipid Rafts Have the Possibility to Migrate to the Opposite Direction of the Initial AC Electric Field Direction.

According to the model, lipid raft should always move in the positive displacement region if the initial sinusoidal AC electric field is toward the positive direction and if there is no constraint on the lipid raft movement. The first half of the sinusoidal electric field (toward the positive direction) brings the lipid raft away from its origin to the positive displacement side, and the second half of the sinusoidal electric field (toward the negative direction) brings the lipid raft back to the origin. If lipid raft does not grow, a full sinusoidal cycle brings the lipid raft back to the origin. If lipid raft grows during the sinusoidal cycle, the lipid raft cannot fully migrate back to the origin since growth always decreases drift velocity. In both situations, lipid raft would always move to the positive side of the initial direction. However, if we consider the existence of a boundary constraint, as other membrane components and the submembranous cytoskeleton can restrict molecule movement (23), lipid rafts can be trapped at the boundary until the AC field changes direction and lipid raft can to move to the negative region.

Figure 4 shows an example that lipid raft displacement can be shifted towards to negative side when different boundary sizes are set. When there is no boundary (Figure 4(a)), lipid raft can move up to 0.25 μm in the first sinusoidal AC cycle. Later, the displacement decreases because lipid raft size increases. As expected, displacement is always in the positive side. Figure 4(b) shows the situation when we set a boundary equal to 0.15 μm. Lipid raft is trapped at the boundary in the first half of the sinusoidal AC cycle. When the field changes direction, lipid raft could travel further than the distance between the boundary and the origin and therefore move to the negative side. Figure 4(c) further shows that the location can be further shifted to the negative side if

the boundary is further reduced to 0.1 μm.

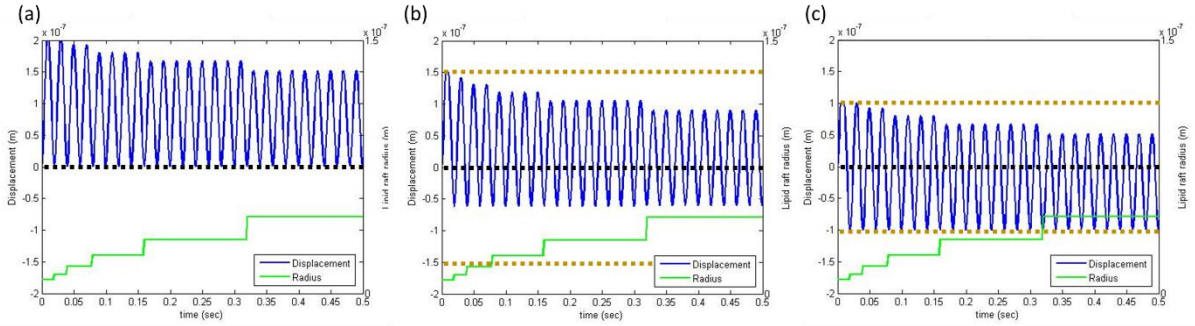

Figure 4. Predicted displacement situations when the maximum displacement constraint is set to be (a) no boundary, (b) 0.15 μm, and (c) 0.1 μm. Brown dashed line: constraint of maximum displacement. The electric field lines are removed for simplification. Symbols, lines and axes are the same as those in Figure 2.

References

1. Tsai C-C, *et al.* (2010) Overexpression of hTERT increases stem-like properties and decreases spontaneous differentiation in human mesenchymal stem cell lines. *J Biomed Sci* 17(1):64.
2. Chu Y-W, *et al.* (1997) Selection of Invasive and Metastatic Subpopulations from a Human Lung Adenocarcinoma Cell Line. *Am J Respir Cel Mol Biol* 17(3):353-360.
3. Danthi P & Chow M (2004) Cholesterol Removal by Methyl-β-Cyclodextrin Inhibits Poliovirus Entry. *J Virol* 78(1):33-41.
4. Carmena MJ, Hueso C, Guijarro LG, & Prieto JC (1991) Cholesterol modulation of membrane fluidity and VIP receptor/effector system in rat prostatic epithelial cells. *Regulatory Peptides* 33(3):287-297.
5. Tsai C-H, Lin B-J, & Chao P-HG (2013) α2β1 integrin and RhoA mediates electric field-induced ligament fibroblast migration directionality. *J Orth Res* 31(2):322-327.
6. Manders EMM, Verbeek FJ, & Aten JA (1993) Measurement of co-localization of objects in dual-colour confocal images. *Journal of Microscopy* 169(3):375-382.
7. McLaughlin S & Poo M-m (1981) The role of electro-osmosis in the electric-field-induced movement of charged macromolecules on the surface of cells. *Biophys J* 34:85-93.
8. Yoshina-Ishii C & Boxer SG (2006) Controlling two-dimensional tethered

vesicle motion using an electric field: interplay of electrophoresis and electro-osmosis. *Langmuir* 22:2384-2391.
9. Han X, *et al.* (2009) Manipulation and charge determination of proteins in photopatterned solid supported bilayers. *Integrative Biology* 1:205-211.
10. Bier M (1959) *Electrophoresis: Theory, Methods, and Applications* (Academic Press, New York).
11. Bird BR, Stewart WE, & Lightfoot EN (1960) *Transport Phenomena* (John Wiley & Sons, Inc., New York).
12. Petrov EP & Schwille P (2008) Translational diffusion in lipid membranes beyond the Saffman-Delbrück approximation. *Biophys J* 94(5):L41-L43.
13. Deen WM (1998) *Analysis of Transport Phenomena* (Oxford University Press).
14. Guigas G & Weiss M (2008) Influence of Hydrophobic Mismatching on Membrane Protein Diffusion. *Biophys J* 95(3):L25-L27.
15. Saffman PG & Delbrück M (1975) Brownian motion in biological membranes. *Proc Natl Acad Sci USA* 72(8):3111-3113.
16. Peters R & Cherry RJ (1982) Lateral and rotational diffusion of bacteriorhodopsin in lipid bilayers: experimental test of the Saffman-Delbrück equations. *Proc Natl Acad Sci USA* 79(14):4317-4321.
17. Bondar OV, Saifullina D, Shakhmaeva I, Mavlyutova I, & Abdullin T (2012) Monitoring of the zeta potential of human cells upon reduction in their viability and interaction with polymers. *Acta Naturae (англоязычная версия)* 4(1 (12)).
18. Jacobson K, Mouritsen OG, & Anderson RG (2007) Lipid rafts: at a crossroad between cell biology and physics. *Nat Cell Biol* 9(1):7-14.
19. Selvi RB, *et al.* (2012) ATP driven clathrin dependent entry of carbon nanospheres prefer cells with glucose receptors. *Journal of nanobiotechnology* 10(1):35.
20. Simons K & Vaz WL (2004) Model systems, lipid rafts, and cell membranes 1. *Annu Rev Biophys Biomol Struct* 33:269-295.
21. Finkelstein E, Chao P-HG, Hung CT, & Bulinski JC (2007) Electric field-induced polarization of charged cell surface proteins does not determine the direction of galvanotaxis. *Cell Motil Cytoskeleton* 64(11):833-846.
22. Merritt EA, *et al.* (1994) Crystal structure of cholera toxin B-pentamer bound to receptor GM1 pentasaccharide. *Protein Sci* 3(2):166-175.
23. Gowrishankar K, *et al.* (2012) Active remodeling of cortical actin regulates spatiotemporal organization of cell surface molecules. *Cell* 149(6):1353-1367.